ADVANCES IN ATMOSPHERIC SCIENCES, VOL. 30, NO. 2, 2013, 315–329

Seasonal and Intraseasonal Variations of East Asian Summer Monsoon Precipitation Simulated by a Regional Air–Sea Coupled Model

FANG Yongjie[1] (房永杰), ZHANG Yaocun*[2] (张耀存)
HUANG Anning[2] (黄安宁), and LI Bo[3] (李 博)

[1]*Beijing Climate Center, China Meteorological Administration, Beijing* 100081

[2]*School of Atmospheric Sciences, Nanjing University, Nanjing* 210093

[3]*Key Laboratory of Radiometric Calibration and Validation for Environmental Satellites, China Meteorological Administration, Beijing* 100081

(Received 22 November 2011; revised 5 June 2012)

ABSTRACT

The performance of a regional air–sea coupled model, comprising the Regional Integrated Environment Model System (RIEMS) and the Princeton Ocean Model (POM), in simulating the seasonal and intraseasonal variations of East Asian summer monsoon (EASM) rainfall was investigated. Through comparisons of the model results among the coupled model, the uncoupled RIEMS, and observations, the impact of air–sea coupling on simulating the EASM was also evaluated. Results showed that the regional air–sea coupled climate model performed better in simulating the spatial pattern of the precipitation climatology and produced more realistic variations of the EASM rainfall in terms of its amplitude and principal EOF modes. The coupled model also showed greater skill than the uncoupled RIEMS in reproducing the principal features of climatological intraseasonal oscillation (CISO) of EASM rainfall, including its dominant period, intensity, and northward propagation. Further analysis indicated that the improvements in the simulation of the EASM rainfall climatology and its seasonal variation in the coupled model were due to better simulation of the western North Pacific Subtropical High, while the improvements of CISO simulation were owing to the realistic phase relationship between the intraseasonal convection and the underlying SST resulting from the air–sea coupling.

Key words: regional air–sea coupled model, East Asian summer monsoon rainfall, climatological intraseasonal oscillation

Citation: Fang, Y. J., Y. C. Zhang, A. N. Huang, and B. Li, 2013: Seasonal and intraseasonal variations of East Asian summer monsoon precipitation simulated by a regional air–sea coupled model. *Adv. Atmos. Sci.*, **30**(2), 315–329, doi: 10.1007/s00376-012-1241-6.

1. Introduction

The summer climate of East Asia is characterized by marked monsoon climate. The complex topography, the strong ocean–continent contrast and air–sea interaction associated with monsoonal activities are the dominant features forcing the East Asian summer monsoon (EASM) climate and its variations (Ding and Chan, 2005). These unique features make EASM prediction a great challenge to the climate research community and require special consideration in designing high-resolution regional climate models (RCMs) to be used in this particular region. Various attempts have been made in the development of RCMs suitable for the simulation of the East Asian climate (Lee and Suh, 2000; Wang et al., 2003; Fu et al., 2005; Zou et al., 2010). Previous results have shown that RCMs are more skillful at resolving land surface heterogeneity and other physical processes and thus can better capture the regional-scale characteristics of climate vari-

*Corresponding author: ZHANG Yaocun, yczhang@nju.edu.cn

ables compared to the more coarse-resolution GCMs (Giorgi and Bates, 1989; Kim and Hong, 2007).

Although significant progress has been made in the area of regional climate modeling, there remain many discrepancies in current RCMs, especially with respect to their relatively low skill in simulating precipitation and its variations on different timescales (Leung et al., 1999; Fu et al., 2005). One of the major uncertainties of current RCMs is the representation of air–sea interaction. Previous studies have found that atmospheric forcing dominates local air–sea interaction over the East Asian coastal oceans in summertime (Wu and Kirtman, 2007). When the observed SST anomalies induced by atmospheric forcing are used to force RCMs, unrealistic atmospheric variability and improper local air–sea relationships appear (Wang et al., 2005; Wu and Kirtman, 2007). Therefore, a two-way coupling between ocean and the regional atmosphere needs to be included in RCMs to properly reproduce the monsoon climate over East Asia.

In recent years, great worldwide efforts have also been made in the development of regional air–sea coupled models, with a focus on the air–sea coupling process in monsoon regions (Aldrian et al., 2005; Ratnam et al., 2009), weather and climate forecasting (Döscher et al., 2002), and extreme climate events (Seo et al., 2007; Vincenzo et al., 2010). There are also some regional coupled modeling studies concerning the EASM (Ren and Qian, 2005; Fang et al., 2010; Li and Zhou, 2010). While improvements are evident in coupled simulations of the EASM, the results of individual regional coupled models are preliminary and vary widely depending on different model components, especially for the atmospheric component (Zou and Zhou, 2011). Moreover, most of the regional air–sea coupled models generally show systematic biases in their simulations of the EASM when compared with observations, such as the overestimation of precipitation over eastern China and the cold bias of SST over East Asian coastal oceans (Ren and Qian, 2005; Fang et al., 2010). Therefore, a more thorough and multifold evaluation of the coupled model's reproduction of the EASM is needed, not only to provide a scientific basis for its further development and improvement, but also to better understand the coupling processes between the East Asian coastal oceans and monsoonal circulations.

In the study reported upon in the present paper, the regional air–sea coupled model developed by Fang et al. (2010), based on the Regional Integrated Environment Model System (RIEMS) and the Princeton Ocean Model (POM), was applied to simulate the climatological variations of EASM rainfall. Climatological EASM rainfall exhibits complex timescales of variation, among which seasonal variation has the most dominant characteristics. The rainy season, contributing to most of the annual water resources in East Asian countries, is strongly controlled by the seasonal evolution of the EASM rainband and associated large-scale circulation (Tao and Chen, 1987; Lau et al., 1988). It is also well known that the climatological intraseasonal oscillation (CISO) is an essential component of the EASM system (Krishnamurti, 1985; Kang et al., 1999), strongly regulating the climatological onset (retreat) and active (break) spells of the EASM (Huang and Sun, 1994; Wang and Xu, 1997; Kang et al., 1999; Mao et al., 2010). Considering the diverse temporal and spatial characteristics of the climatological variations of the EASM, a reasonable simulation of the seasonal and intrseasonal variations of EASM rainfall by RCMs is therefore important for the dynamical forecasting of the EASM, as well as climate prediction over China.

The purpose of our study was to evaluate the performance of the regional air–sea coupled model and investigate whether the air–sea coupling can improve the simulation of climatological variations of EASM rainfall compared to a climate model without air–sea coupling. The remainder of the paper is organized as follows. Section 2 gives a description of the oceanic and atmospheric models, the numerical experiment schemes, and the dataset used. A detailed analysis of the numerical results is presented in section 3. Finally, the main findings and conclusions from this work are summarized in section 4.

2. Model description, experiments and dataset

2.1 *Atmosperhic and oceanic components*

The atmospheric component of the coupled climate model system is the Regional Integrated Environment Model System (RIEMS), which was developed by the global change System for Analysis, Research and Training Regional Center for Temperate East Asia (START TEA) (Fu et al., 2000). It is a primitive equation, grid-point-limited area model with hydrostatic compressible balance written in a terrain-following coordinate system. The RIEMS is an augmented version of the National Center for Atmospheric Research (NCAR) Penn State Mesoscale Model, MM5. A number of physical parameterizations have been employed in the RIEMS, including a widely applied land surface scheme [the Biosphere–Atmosphere Transfer Scheme (BATS; Dickinson et al., 1986)], a Holtslag explicit planetary boundary layer formulation (Holtslag et al., 1990), a Grell cumulus parameterization (Grell, 1993), and a modified radiation package (CCM3). The

RIEMS is currently participating in the Regional Climate Model Intercomparison Project (RMIP) to simulate the regional climate in Asia (Fu et al., 2005). Analysis of its simulation results contributing to RMIP has shown that it has a moderate ability in simulating the mean climate state, extreme events, and climate changes over East Asia (Wu et al., 2004; Xiong et al., 2006).

The oceanic component of the coupled model system is the POM, which was developed in the late 1970s by Mellor's group at Princeton University (Blumberg and Mellor, 1987). It is a 3-D, free-surface, primitive equation model using Arakawa-C grid staggering and a sigma coordinate in the vertical. Vertical diffusivities and viscosities are derived from the Mellor-Yamada turbulent closure submodel (Mellor and Yamada, 1982), which yields realistic surface and bottom Ekman layers. Horizontal diffusivities and viscosities are parameterized by the Smagorinsky relation to horizontal resolution and dynamics (Smagorinsky, 1963). The version of POM used in this study was the result of improvements made by Chu and Chang (1997) and Qian et al. (1998), and has shown good performance in simulating the intraseasonal, seasonal, and annual variation of SST and circulation in the East Asian coastal regions (Zhang and Qian, 1999; Chu et al., 2001). Earlier studies demonstrated that this version of POM can be used to examine the responses of the regional ocean to the monsoon climate (Ren and Qian, 2005; Zou and Zhou, 2011).

2.2 *Regional air–sea coupled climate model system*

In the regional air–sea coupled climate model system, RIEMS and POM share the same model domain, which covers most of the East Asian monsoon region centered at 24°N, 121°E (Fig. 1). The horizontal resolution of both the atmospheric and oceanic models is 60 km. RIEMS has 18 vertical layers with a model top pressure of 50 hPa. POM adopts 16 vertical sigma levels with approximately eight layers in the upper 100 m of water.

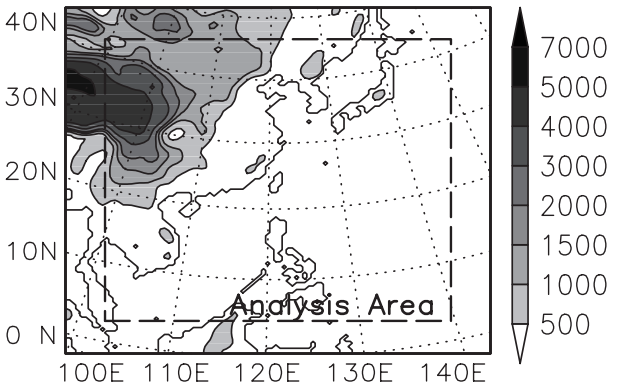

Fig. 1. Regional model domain and topography height (m). Dashed box denotes the analysis area.

The linkage between the oceanic and atmospheric components is established by a flux–SST coupler in the regional air–sea coupled model system. The coupler's task is to transfer the surface wind stress and surface heat fluxes (downward net shortwave and longwave radiation, sensible heat and latent heat fluxes) calculated in RIEMS to POM and feed back RIEMS the SST calculated in POM. The exchange of these variables between atmospheric and oceanic components of the regional air–sea coupled model is carried out every six hours during the numerical integration. At the lateral open ocean boundaries, a combination of radiation and relaxation conditions were implemented for the present study (Barnier et al., 1998). The air-sea coupling does not introduce correction of heat and momentum fluxes.

2.3 *Numerical experiments*

In this work, two numerical experiments were carried out. The first, CTRL_EXP, used uncoupled RIEMS, and the other, CPL_EXP, used the regional air–sea coupled model. NCEP/NCAR reanalysis data at 6-h intervals (Kalnay et al., 1996) provided the atmospheric initial and lateral boundary conditions in CTRL_EXP and CPL_EXP. In CTRL_EXP, the oceanic boundary forcing was offered by weekly mean global SST (GISST) data (Reynolds et al., 2002). The uncoupled RIEMS was carried out from 25 April to 1 September in each year during the period 1985–2004.

In CPL_EXP, the oceanic boundary forcing was provided by the oceanic component of the regional air–sea coupled model. The precoupling ocean spin-up integration before running the coupled model included two steps. In the first step, POM was driven by the NCEP/NCAR monthly wind stress and surface heat fluxes (latent and sensible heat fluxes, downward net shortwave and longwave radiation) averaged over 1985–2004 were integrated for 1 yr from an initial resting state. The lateral boundary conditions were derived from the monthly Levitus climatological salinity and temperature (Levitus, 1984). In the second step, POM was continuously integrated from 1 January to 25 April forced by NCEP/NCAR reanalysis data in each year over 1985–2004, respectively. After these two steps, the whole ocean reached a relatively equilibrium and realistic state. Then, the regional air–sea coupled climate model whose oceanic components takes the outputs of the second step as the initial conditions, was run interactively from 25 April to 1 September for each year from 1985–2004.

2.4 *Methodology and dataset*

Both CTRL_EXP and CPL_EXP outputted daily mean data. Each experiment obtained model results for 20 summers (1985–2004). To eliminate high-frequency signals, all daily mean data were first averaged to pentad mean data before analysis. To reveal the spatial and temporal patterns of summer monsoon rainfall variation, EOF analysis was applied to pentad mean precipitation anomalies from the observation and simulations. The power spectra from each of the 20-yr pentad rainfall were averaged to identify the mean timescale of the CISO. This timescale was then isolated by applying a Lanczos filter (Duchon, 1979) to the pentad mean rainfall during May to August.

For model validation, various observational data were analyzed for May–August over the period 1985–2004. The pentad mean rainfall data were derived from the Climate Prediction Center Merged Analysis of Precipitation (CMAP; Xie and Arkin, 1997). NCEP/NCAR reanalysis data were used to validate the modeled atmospheric circulation in the interior of the model domain shown in Fig. 1.

3. Results

3.1 *Climatological mean of the EASM rainfall*

Since the distribution of EASM rainfall and its variations is closely related to SST anomalies over East Asian coastal oceans (Ding and Chan, 2005), we firstly examine the SST distribution simulated by the regional air–sea coupled model. Figure 2 shows the spatial pattern of the observed and modeled 20-yr summer mean SST. The observed SST (Fig. 2a) over 29°C was located in the south of 20°N, including the South China Sea (SCS) and the Northwest Pacific. The regional air–sea coupled model successfully reproduced the higher SST over the SCS (Fig. 2b). However, compared with the observation, cold biases in the modeled SST occurred in part of the western Pacific warm pool. Simulated SST greater than 29°C retreated to south of 10°N, and this bias was also evident in some previous regional coupled models (Ren and Qian, 2005; Zou et al., 2010). Fang et al. (2010) pointed out that the SST biases were due to the adjustment of SST to the errors of surface heat fluxes simulated by the RIEMS in the coupled system.

Figure 3 shows the observed and modeled 20-yr climatological summer mean precipitation. As shown in Fig. 3a, the greatest intensity of the observed summer mean precipitation was located along 15°N over the Philippine Sea and SCS. It should also be noted that three large rainfall centers were located over eastern China, the Korean peninsula, and Japan, respectively, which corresponded to the EASM rainband. These main features were generally reproduced by CPL_EXP (Fig. 3c) and CTRL_EXP (Fig. 3b), but the rainfall amount was underestimated over the whole East Asian coastal oceans area and overestimated over eastern China, respectively (Figs. 3b, c). Other RCMs have shown similar biases, which are probably associated with the cumulus convective parameterization scheme (Leung et al., 1999; Yhang and Hong, 2008). CPL_EXP had a spatial pattern correlation coefficient of 0.36 with CMAP data, while CTRL_EXP returned a value of 0.28 (Table 1). The difference in rainfall between CPL_EXP and CTRL_EXP (Fig. 3d) indicates that the inclusion of air–sea interaction in the coupled model improves rainfall simulation, e.g. rainfall modeled by the coupled model increased over almost the whole Northwest Pacific and reduced over North China (Fig. 3d), and this simulation was in better agreement with the observation than the uncoupled RIEMS.

3.2 *Variation of the climatological summer precipitation during May to August*

The variation of the modeled climatological summer precipitation from CTRL_EXP and CPL_EXP were examined by analyzing the 20-yr mean pentad data during May to August. As shown in Fig. 4, the standard deviation gives the amplitude of the precipitation variation in summer. The standard deviation of observed precipitation (Fig. 4a) showed a similar pattern to its mean state (as shown in Fig. 2a), with large variations located over the Philippine Sea, SCS, eastern China, the Korean peninsula, and Japan. Both CTRL_EXP and CPL_EXP captured this spatial pattern, but the amplitude of the modeled variation was weaker (stronger) over the Philippine Sea and SCS (eastern China) than the observation. Compared with the CTRL_EXP, CPL_EXP reduced (increased) the amplitude of the precipitation variation over east-

Table 1. The correlation coefficients of summer mean rainfall, CISO intensity, standard deviation of EASM rainfall over the analysis area (see Fig. 1), and PCs of the first two EOF modes of EASM rainfall between the simulations and observation.

	Mean rainfall	Standard deviation	PC1	PC2	CISO intensity
CTRL_EXP	0.28	0.37	0.70	0.50	0.09
CPL_EXP	0.36	0.43	0.81	0.68	0.30

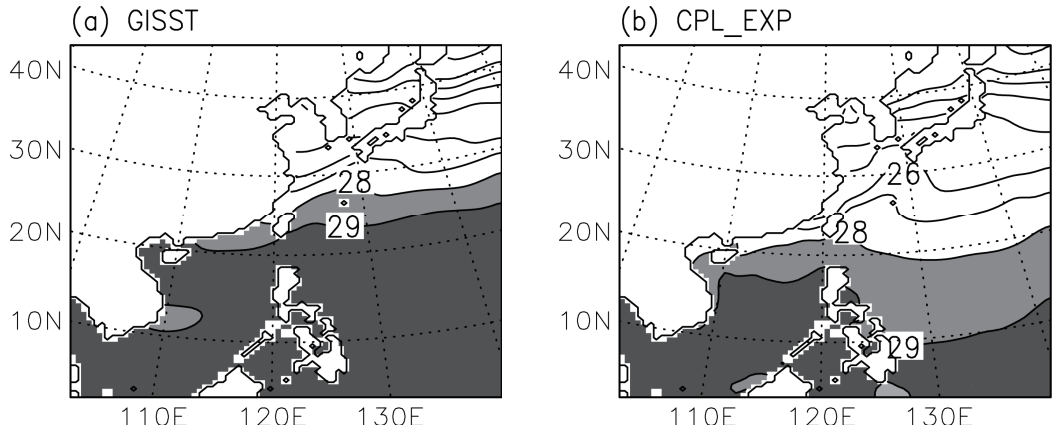

Fig. 2. The climatological summer mean SST (°C) from (a) GISST and (b) CPL_EXP. Regions with SST greater than 28°C are shaded.

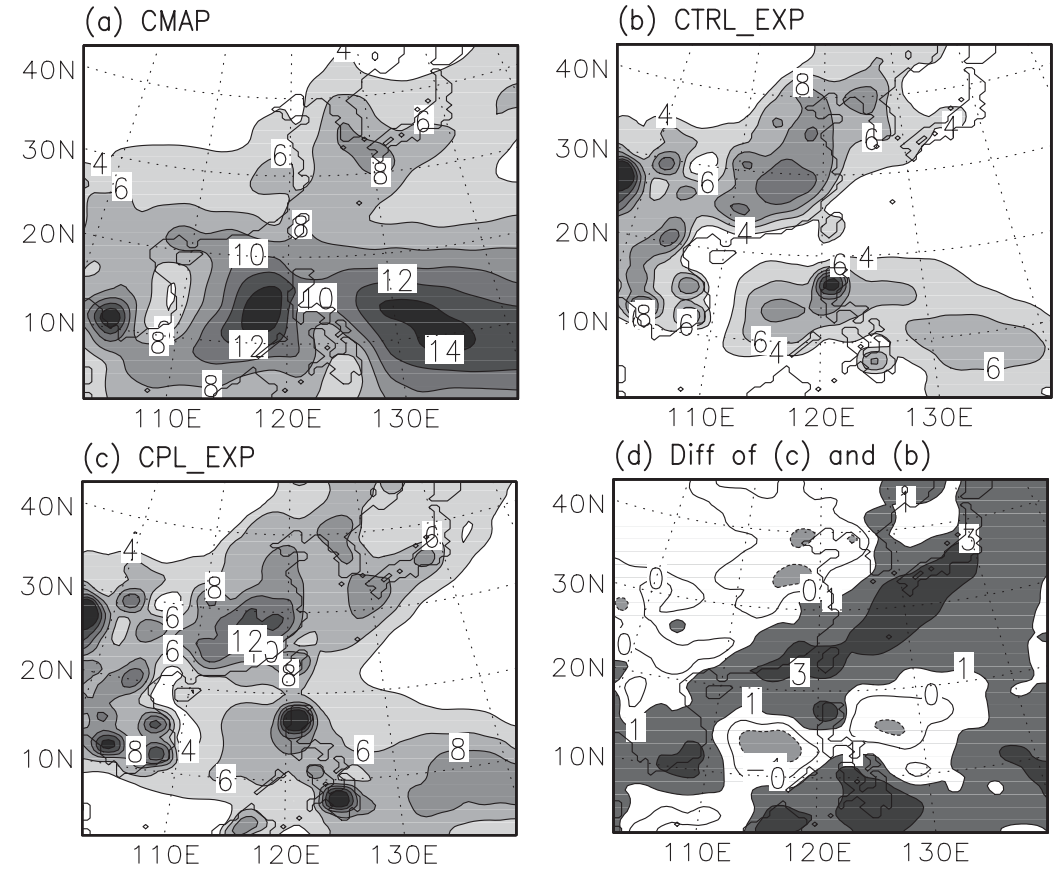

Fig. 3. The climatological summer mean precipitation (five-point smoothing, mm d^{-1}) from (a) CMAP, (b) CTRL_EXP, and (c) CPL_EXP. (d) is for the difference in summer precipitation between CPL_EXP and CTRL_EXP. Regions with precipitation greater than 4 mm d^{-1} in (a–c) and the difference in precipitation greater (less) than 1 mm d^{-1} in (d) are dark (light) shaded.

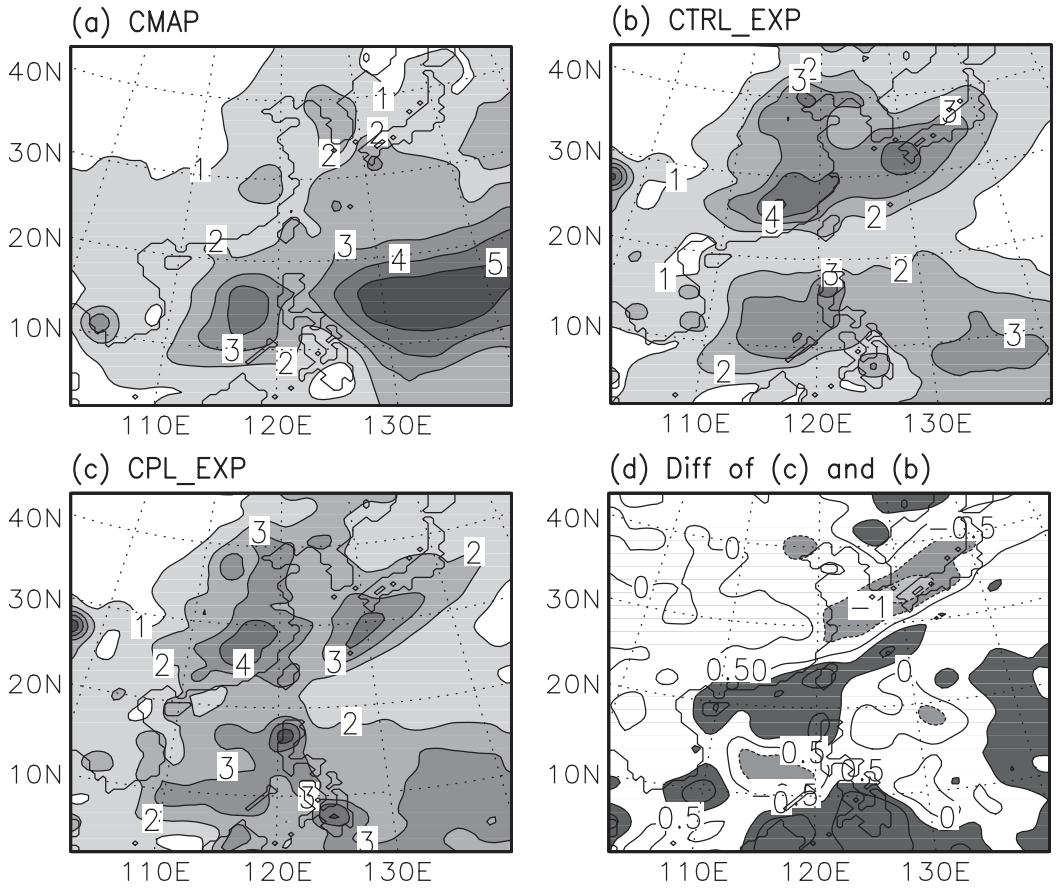

Fig. 4. The standard deviation of climatological variations of pentad precipitation (mm d^{-1}) from May to August from (a) CMAP, (b) CTRL_EXP, and (c) CPL_EXP. (d) is for the difference in precipitation standard deviation between CPL_EXP and CTRL_EXP. Regions with the precipitation standard deviation greater than 4 mm d^{-1} in (a–c) and the difference in precipitation standard deviation greater (less) 0.5 mm d^{-1} in (d) are dark (light) shaded.

ern China and Japan (Philippine Sea) (Fig. 2d), indicating a general improvement in the RIEMS model performance by coupling with the ocean model.

The principal modes of the 20-yr climatological EASM rainfall during May to August were examined using the EOF analysis method. Figure 5 displays the first EOF mode of the modeled and observed precipitation. The spatial pattern of the first EOF mode of the observed precipitation (Fig. 5a) showed a negative anomaly belt extending from South China northeastward to the Northwest Pacific and southern Japan and two large positive anomaly regions located along the SCS–Philippine Sea and the North China–Far East, respectively. This mode, accounted for 54%, 35%, and 30% of the total variance in the observation, CTRL_EXP, and CPL_EXP respectively, representing the seasonal evolution of the broad-scale EASM. Both CTRL_EXP and CPL_EXP simulated the pattern of the first EOF mode well, comparable to the observation in terms of the position of the precipitation anomaly centers (Figs. 5b, c). Note that the magnitude of the precipitation anomalies across the East Asian coastal oceans, especially in the Philippine Sea, was somewhat better simulated in CPL_EXP than that in CTRL_EXP. The corresponding principal components (PC1s) are shown in Fig. 5d. The correlation coefficient of the PC1 between CPL_EXP and the observation was higher than that between CTRL_EXP and the observation (0.81 vs 0.70; Table 1). In addition, the PC1 of CTRL_EXP results (Fig. 5d) showed a delayed onset of monsoon rainfall, with the turning point from negative to positive phase being in early July, while in CPL_EXP and in the observation it occurred in late June and mid-June, respectively.

The second EOF mode of the observed rainfall

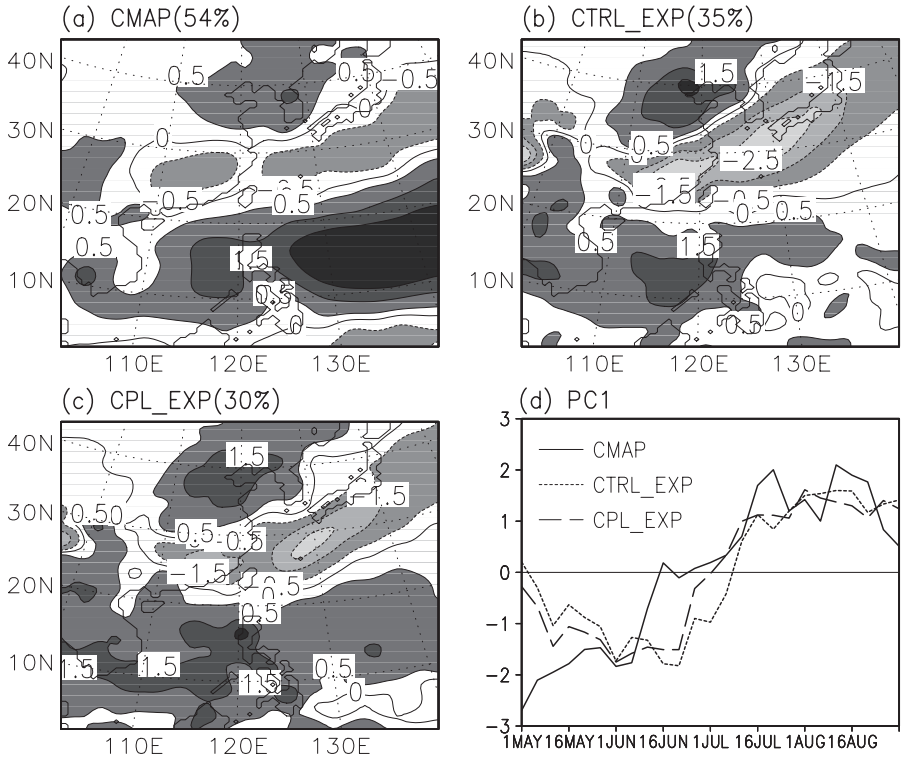

Fig. 5. The first EOF mode of the climatological pentad precipitation during May to August from (a) CMAP, (b) CTRL_EXP, and (c) CPL_EXP. The PC of the first EOF mode is shown in (d).

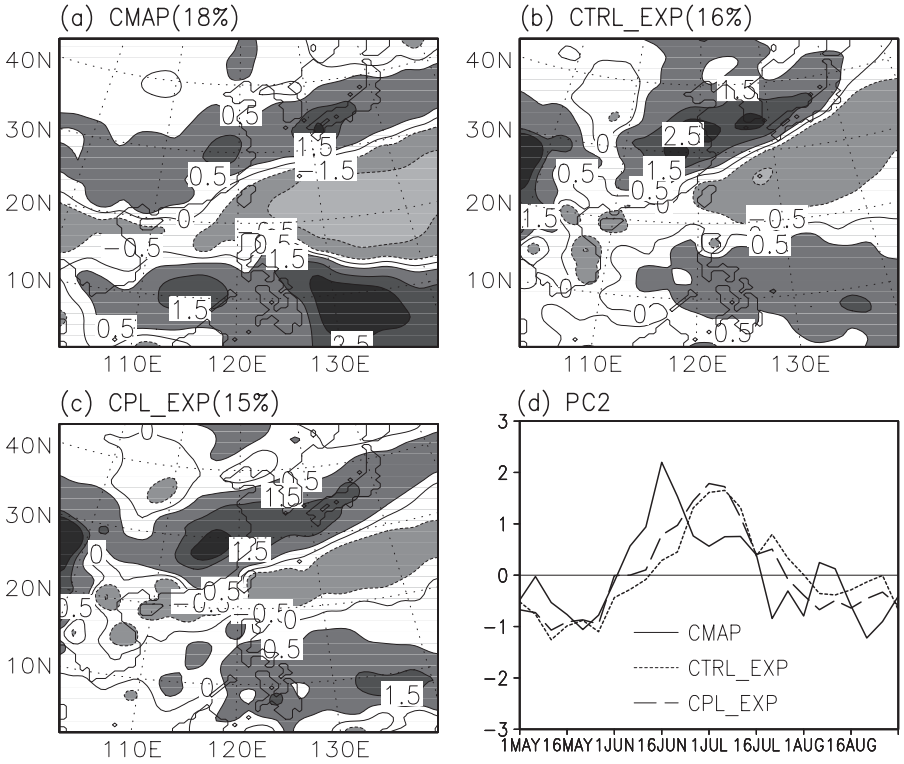

Fig. 6. As in Fig. 5, but for the second EOF mode and the associated PC.

was characterized by a negative anomaly belt over the Northwest Pacific with two positive anomaly belts located on its northwest and south sides, respectively (Fig. 6a). Both CTRL_EXP and CPL_EXP captured the observed pattern of the second EOF mode, and reproduced the positive anomalies belt associated with the Meiyu-Baiu rainband extending from central China to Japan particularly well (Figs. 6b, c). However, the negative anomalies over the Northwest Pacific in both simulations were underestimated compared with the observation. The associated PC2 shown in Fig. 6d indicates that the Meiyu-Baiu rainband prevailing from early June to mid-July was captured in both CTRL_EXP and CPL_EXP. Similar to the PC1, comparison of PC2 between the simulation and observation indicates a delayed onset of the monsoon rainfall in both CTRL_EXP and CPL_EXP. However, CPL_EXP was in better agreement with the observation than CTRL_EXP.

3.3 *CISO of the EASM rainfall*

The performance of the coupled model in simulating CISO of the EASM rainfall in terms of its dominant period, intensity, and propagation will be evaluated in this section. The dominant periodicities of CISO of rainfall over the EASM region (20°–45°N, 110°–140°E) were identified through the spectrums of 20-yr mean pentad precipitation during May to August. The CISO of the observed precipitation had a major spectral peak on day 30 (Fig. 7a). It can be seen that both CTRL_EXP and CPL_EXP showed significant skill in reproducing the 30-day peak, which was well above the 95% confidence level for the reference red noise spectrum (Figs. 7a–c). In the following analyses, the CISO signal was extracted from the climatological pentad rainfall data using a 6–12 pentad (30–60 day) Lanczos filter (Duchon, 1979).

Figure 8 shows the spatial distribution of the CISO intensity for the modeled and observed EASM precipitation, which is defined as the percentage of the variance of CISO to the total variance of pentad rainfall. The observed large value belt of CISO intensity extended from southeastern China to Japan with maximum centers over the Yangtze River valley and Japan. Another large center of CISO intensity can be found over the oceanic region north of 20°N (Fig. 8a). CTRL_EXP failed to reproduce the main distribution of the CISO intensity. For instance, the amplitude of CISO was weaker over the whole EASM region and the centers of large values were positioned more northward than the observation (Fig. 8b). Compared with CTRL_EXP, the amplitude of CISO in CPL_EXP was significantly enhanced over most of the EASM region, and slightly reduced over the Northwest Pacific along 10°–20°N (Fig. 8d), similar to the observation (Fig. 8c). Meanwhile, the spatial pattern correlation coefficient of CISO intensity between CPL_EXP and the observation was 0.30, which was obviously higher than that between CTRL_EXP and the observation, which had a value of 0.09 (Table 1).

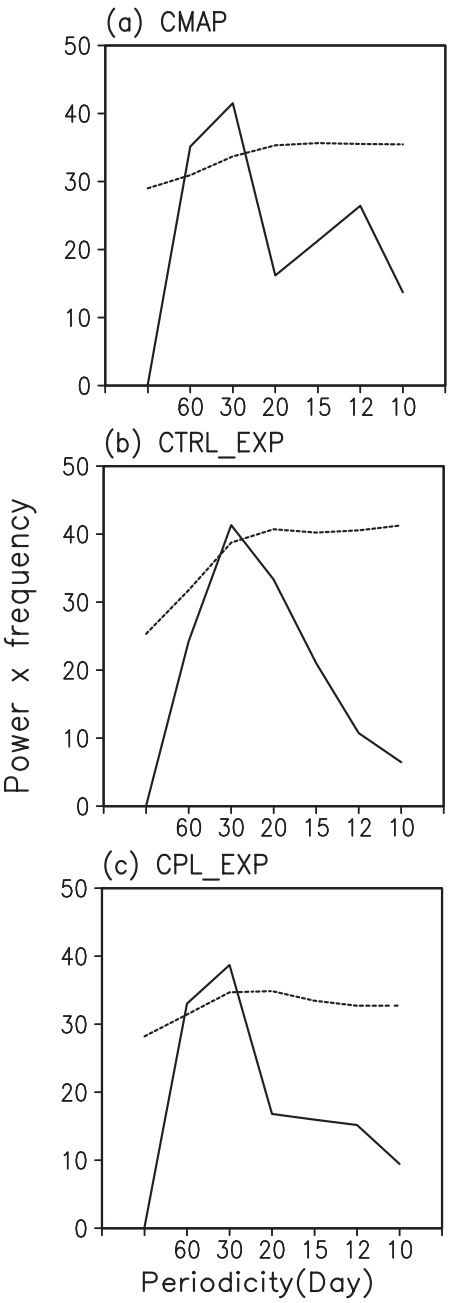

Fig. 7. Power spectrums of the CISO over the EASM region from (a) CMAP, (b) CTRL_EXP, and (c) CPL_EXP. Dashed lines denote that the confidence level is greater than 95% against red noise.

The time–latitude cross sections of the CISO com-

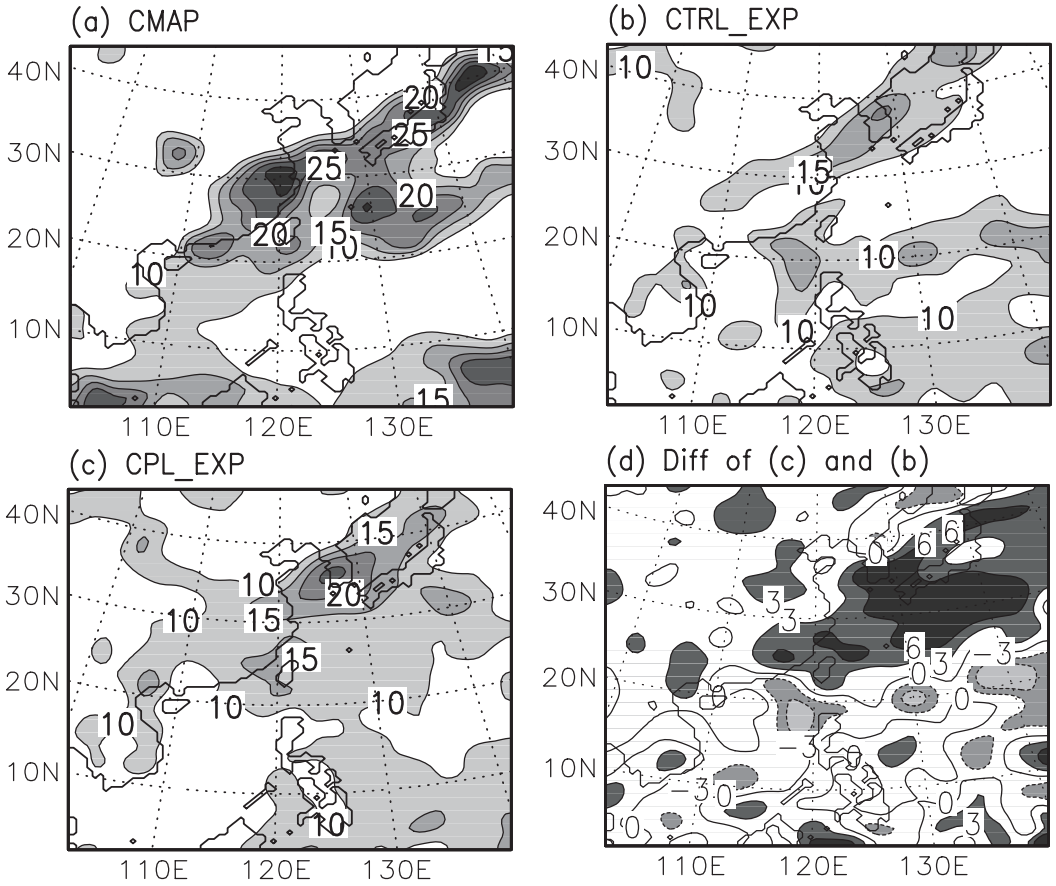

Fig. 8. Distribution of the CISO intensity (%) from (a) CMAP, (b) CTRL_EXP, and (c) CPL_EXP. (d) is for the difference in CISO intensity between CPL_EXP and CTRL_EXP. The CISO intensity is denoted as percentage of variance of CISO to the total variance of the pentad mean rainfall from May to August. Regions with CISO intensity greater than 10% in (a–c) and the difference in CISO intensity greater (less) 3% in (d) are dark (light) shaded.

ponent of precipitation averaged along 125°–135°E from CMAP, CTRL_EXP, and CPL_EXP are presented in Fig. 9. During the period from 1 May to 1 September, three CISO events can be identified in the observation (Fig. 9a). The strongest event, appearing in early May, propagated northward from the Northwest Pacific to the Japan Sea, which was associated with the climatological onset of the EASM. Both CTRL_EXP and CPL_EXP captured the first two events but failed to reproduce the third event, which appeared in late August over the Northwest Pacific (Figs. 9b, c). It should also be noted that the propagating speed of CISO events in both CTRL_EXP and CPL_EXP was slower than the observation (Figs. 9b, c). Compared with CTRL_EXP, CPL_EXP showed notable improvements in the simulation of CISO northward propagation. For example, the signal of the first CISO event in CTRL_EXP was weaker to the south of 30°N, while it was more realistic in CPL_EXP. The second CISO event in CTRL_EXP was confined to the south of the Northwest Pacific (Fig. 9b), whereas it propagated obviously northward to 30°N in CPL_EXP, which was consistent with the observation (Fig. 9c).

3.4 *Possible explanations for the improvement of the climatological variations of EASM rainfall simulated in CPL_EXP*

As mentioned above, the regional air–sea coupled climate model showed better performance in simulating the location and intensity of the EASM rainfall climatology and its climatological seasonal and intraseasonal variations compared with the uncoupled RIMES. This indicates that the inclusion of the air–sea coupling in RIEMS is necessary for EASM rainfall simula-

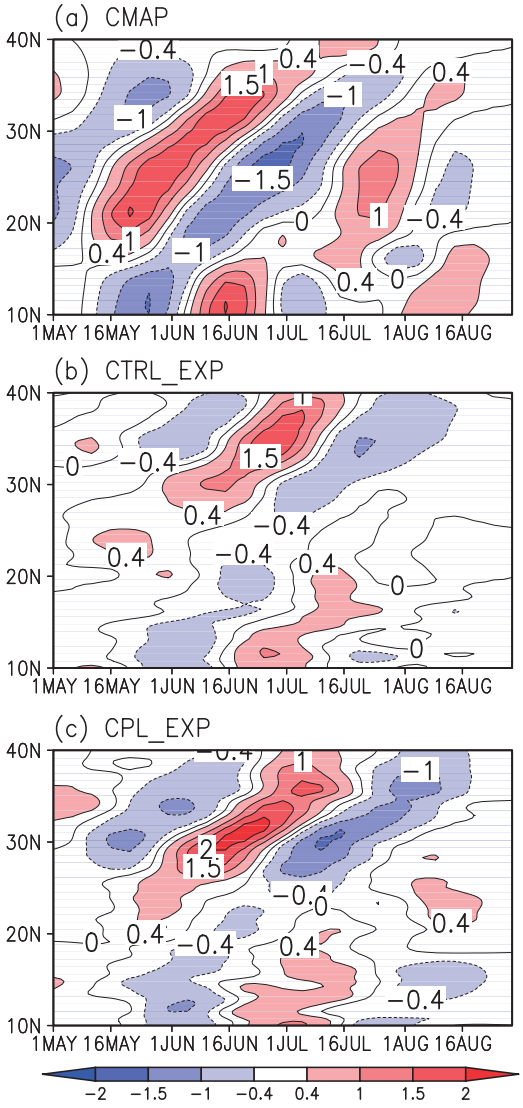

Fig. 9. Time–latitude cross sections of the climatological intraseasonal component of precipitation (mm d^{-1}) averaged along 125°–135°E from (a) CMAP, (b) CTRL_EXP, and (c) CPL_EXP.

tion. In this section, we explore the reasons for the improvements in the climatological variations of the EASM rainfall modeled by the coupled system.

3.4.1 *Possible explanations for the improvement of seasonal variation of EASM rainfall simulated in CPL_EXP*

It is well known that the seasonal variation of EASM rainfall is associated with the intensity, structure and location of the western North Pacific Subtropical High (WNPSH) (Huang and Yu, 1962; Tao and Chen, 1987). Therefore, in this section, the observed and simulated climatological summer mean geopotential height and the associated water vapor transport at 850 hPa are examined. As shown in Fig. 10, both CTRL_EXP and CPL_EXP captured the gross pattern of the WNPSH and the low-level water vapor transport over the EASM region (Figs. 10b, c). However, the simulated WNPSH in CTRL_EXP was stronger and extended more westward than the observation, yielding underestimated (overestimated) rainfall over the East Asian coastal oceans (eastern China) (shown in Figs. 3b, c). Compared to CTRL_EXP, the 850-hPa geopotential height in CPL_EXP was weaker over most parts of East Asia and the Northwest Pacific, more consistent with the NCEP/NCAR reanalysis data (Fig. 10c). Accompanied with the change in the WNPSH (Fig. 10d), the low-level southwesterlies in CPL_EXP were enhanced over the SCS and Northwest Pacific (figure not shown), resulting in strengthened transportation of warm moist air from the SCS and western Pacific to eastern China and the Northwest Pacific (Fig. 10d). Therefore, the rainfall climatology (see Fig. 3d) was enhanced over most of the EASM region.

The improvement of WNPSH simulation in CPL_EXP might be associated with the change in the net sea surface heat flux by coupling air–sea interactions compared with CTRL_EXP. Figure 11a gives the time–latitude of cross sections of the difference in the net sea surface heat flux (upward is positive) averaged along 125°–135°E between CPL_EXP and CTRL_EXP. It is shown that the net sea surface heat flux in CPL_EXP over the Northwest Pacific was increased during the whole simulation period compared with CTRL_EXP, partly due to the regional air–sea coupling (Fu et al., 2005; Fang et al., 2010). This change of the net sea surface heat flux may have warmed the low-level air by altering the heating rate of the atmosphere (Fig. 11b), and consequently resulted in the weaker and eastward-located WNPSH in the coupled model, which was in better agreement with the observation (Fig. 10c).

Another notable improvement in CPL_EXP was the earlier onset of the EASM rainband associated with the first two leading EOF modes compared with that in CTRL_EXP. This should also be associated with the improvement of WNPSH simulation. The eastward-located WNPSH in CPL_EXP (Fig. 10c) indicates that the SCS was more liable to be dominated by the westerly or southwesterly on the west flank of the WNPSH, instead of the easterly on its south side. The enhanced westerly located south of 20°N (Fig. 11c) might have led to an earlier shift from easterly to westerly over the SCS, which marks the onset of the EASM (Wang et al., 2004). As a result, the associated EASM rainband simulated by the regional

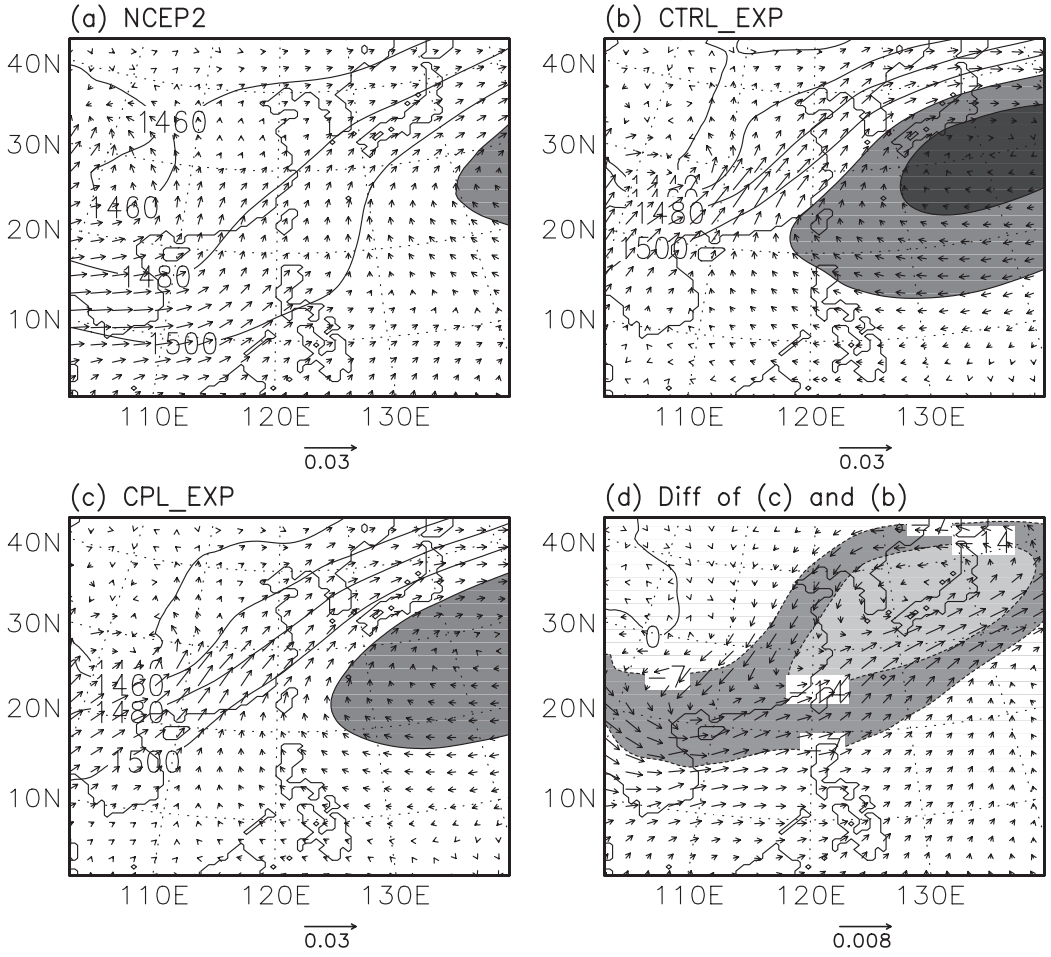

Fig. 10. Summer 850-hPa water vapor transport (kg m^{-1} s^{-1}) and geopotential height (gpm) for: (a) NCAR/NCEPA reanalyses, (b) CTRL_EXP, and (c) CPL_EXP. (d) is for the differences in the summer 850-hPa water vapor transport and geopotential height between CPL_EXP and CTRL_EXP. Regions with geopotential height greater than 1520 gpm in (a–c) and the difference in geopotential height less than −7 gpm in (d) are shaded.

air–sea coupled model displayed an earlier onset than that simulated by the uncoupled RIEMS.

3.4.2 *Possible explanations for the improvement of CISO of EASM rainfall simulated in CPL_EXP*

The most remarkable improvement of CISO of EASM rainfall simulated in CPL_EXP was the stronger intensity of the northward-propagating CISO. This might be associated with the air–sea coupling process in the coupled model, which has been found and confirmed in many previous studies (Fu et al., 2003; Lin et al., 2010). In the observation and CPL_EXP, the negative wind speed led to positive convection in about one–two pentads (Fig. 12a), indicating the decrease of low level wind speed to the north of the convection center. The reduced surface evaporation (Fig. 12b) associated with the wind–evaporation feedback (Wu and Kirtman, 2007), along with the enhanced shortwave radiation (figure not shown) due to the cloud–radiation feedback (Wu and Kirtman, 2007), may have resulted in positive SST anomalies to the north of the convection center. The positive (negative) SST anomalies in CPL_EXP, therefore, systematically led (lagged) convection by about 2 pentads with a correlation coefficient of about 0.6 (−0.6), which agreed well with the observation (Fig. 12c).

The high correlations between SST and low-level air temperature (Fig. 12d), as well as SST with moisture convergence (Fig. 12e), in the observation and

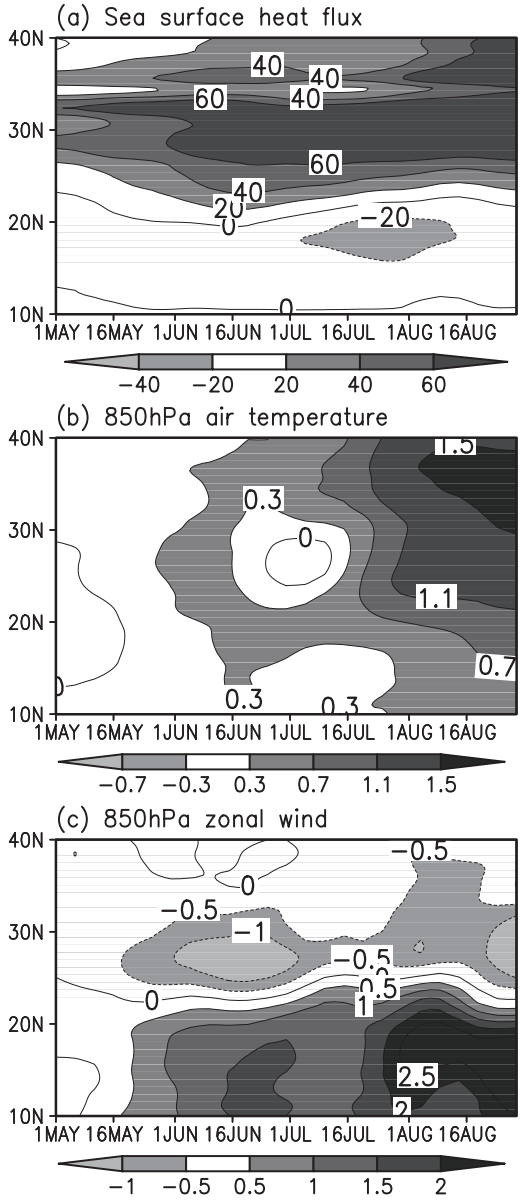

Fig. 11. The time–latitude cross sections of the differences between CPL_EXP and CTRL_EXP in (a) sea surface heat flux (W m^{-2}) and (b) 850-hPa air temperature (K) averaged along 125°–135°E, and in (c) 850-hPa zonal wind (m s^{-1}) averaged along 110°–120°E.

CPL_EXP imply that the warm SST would in turn have fed back positively to the convection. The enhanced convective instability and boundary layer moisture convergence may then have contributed greatly to the northward propagation of the convection (Jiang et al., 2004). In CTRL_EXP, however, SST was only a boundary forcing for the atmosphere; it could not have fed back to the convection. The weak correlation between SST and precipitation (Fig. 12c), low-level air temperature (Fig. 12d) and moisture convergence (Fig. 12e) suggests that the northward-propagating CISO in the uncoupled RIEMS run was not closely tied to the underlying SST as in the coupled run, which may have been the fundamental cause for the weaker northward propagation of CISO in CTRL_EXP (Fig. 9b).

4. Summary and discussion

In this work, the performance of a regional air–sea coupled model system consisting of RIEMS and POM was evaluated in simulating the seasonal and intraseasonal variations of EASM rainfall. Two experiments, named CTRL_EXP and CPL_EXP, were set by running the uncoupled RIEMS and the coupled regional air–sea coupled climate model, respectively. Each experiment was carried out from 25 April to 1 September in each year over the period 1985–2004. The simulation results from the coupled model have been analyzed, with a comparison of those from the uncoupled RIEMS and the observation. The main findings can be summarized as follows:

(1) The coupled model simulated reasonably well the climatological SST and rainfall distribution over the EASM region. While the simulated SST showed cold biases over part of the western Pacific warm pool, the rainband location and intensity simulated by the coupled model were more reasonable than those modeled by the uncoupled RIEMS. We also found that the coupled model reproduced the larger amplitude of the climatological variations of rainfall over the Philippine Sea, SCS, and East Asia with greater skill than the uncoupled RIEMS. The first two EOF modes of the EASM rainfall represent the seasonal march of the broad-scale monsoon and development of the Meiyu-Baiu rain band. Both the coupled model and the uncoupled RIEMS captured the spatial patterns of the first two EOF modes. However, the coupled model showed a more reasonable performance in capturing the corresponding PC of the first two EOF modes (e.g. the time of phase switching) than the uncoupled RIEMS.

(2) The coupled model was found to be able to broadly capture the dominant periods of the CISO of EASM rainfall, with a major spectral peak appearing around 30 days, and simulated a stronger CISO than the uncoupled RIEMS over most of East Asia, similar to that in the observations. The northward propagations of CISO were also better simulated in the coupled model compared to the uncoupled RIEMS.

(3) Compared with the uncoupled RIEMS, improvements in the simulation of the seasonal variation

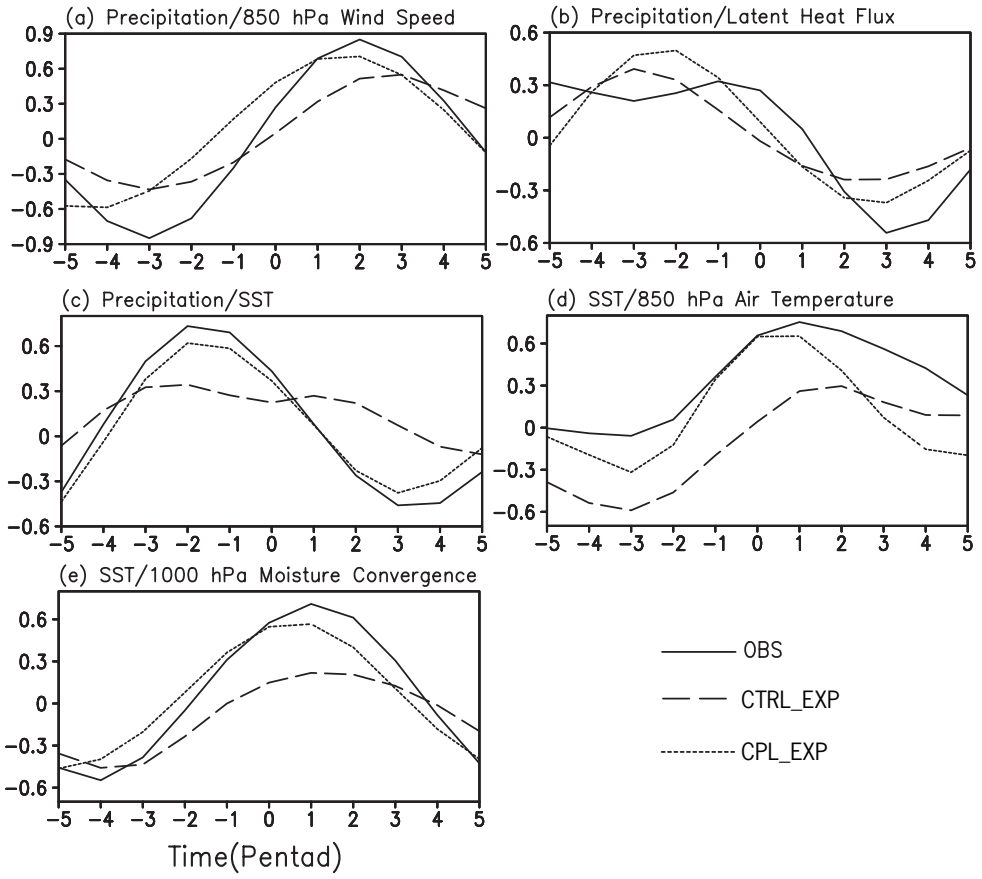

Fig. 12. The lag correlations, averaged over part of the East Asian coastal oceans (20°–30°N, 125°–135°E), between intraseasonal rainfall and (a) 850-hPa wind speed, (b) surface latent heat flux, and (c) SST. (d) and (e) are the same as (a), but for correlations between intraseasonal SST and 850-hPa air temperature and 1000-hPa moisture convergence, respectively.

of EASM rainfall were found in the coupled model, such as the earlier onset of the EASM rainband and enhanced rainfall over most of East Asia, which were found to be associated with better simulation of the WNPSH in CPL_EXP. In addition, the air–sea coupling in the coupled model resulted in a realistic relationship between intraseasonal convection and the underlying SST, which is suggested to be responsible for the improvement in CISO simulation, especially in terms of northward propagation.

In summary, coupling RIEMS with the POM offers an effective strategy to improve the simulation of monsoon rainfall in East Asia. Since the above conclusion is merely based on the results from one regional air–sea coupled model, more coupled models with a variety of RCMs and ocean models need to be developed for EASM rainfall simulation. Moreover, although simulations made by the coupled system were more realistic, the comparison between the coupled model and the uncoupled RIEMS demonstrated that there are similar biases in the uncoupled RIEMS, signifying that the biases present in the RIEMS have a great influence on the performance of the coupling system. From this point, updating the cloud and radiation processes and cumulus convection parameterization, which are closely related to the rainfall simulation, may be an important step for the future development of RIEMS. The results obtained in this study are preliminary, and additional analysis is underway to deepen our understanding of the coupled model and to provide further insights into the regional air–sea coupled model system.

Acknowledgements. This work was supported by the National Natural Science Foundation of China (Grant No. 41105069) and the National Basic Research Program of China (973 Program) (Grant Nos. 2010CB951903 and 2011CB952002). We are grateful to the anonymous review-

ers for their useful suggestions and comments.

REFERENCES

Aldrian, E, D. V. Sein, D. Jacob, L. D. Gates, and R. Podzun, 2005: Modeling Indonesian rainfall with a coupled regional model. *Climate Dyn.*, **25**, 1–17.

Barnier, B., P. Marchesiello, A. P. de Miranda, J. M. Molines, and M. Coulibaly, 1998: A sigma-coordinate primitive equation model for studying the circulation in the South Atlantic. Part I: Model configuration with error estimates. *Deep–Sea Res.*, **45**, 543–572.

Blumberg, A. F., and G. L. Mellor, 1987: A description of a three-dimensional coastal ocean model. Vol. 4, *Three Dimensional Coastal Ocean Models*, N. S. Heaps, Ed., American Geophysical Union, Washington DC, 1–16.

Chu, P. C., and C. P. Chang, 1997: South China Sea warm pool in boreal spring. *Adv. Atmos. Sci.*, **14**(2), 195–206, doi: 10.1007/s00376-997-0019-8.

Chu, P. C., S. H. Lu, and Y. C. Chen, 2001: Evaluation of the Princeton Ocean Model using South China Sea Monsoon Experiment (SCSMEX) data. *J. Atmos. Oceanic Technol.*, **18**, 1521–1539.

Dickinson, R. E., A. Henderson-Sellers, P. J. Kennedy, and M. Wilson, 1986: Biosphere-Atmosphere Transfer Scheme (BATS) for the NCAR Community Climate Model. Tech. Note, NCAR/TN-275+STR, National Center for Atmospheric Research, CO, 69pp.

Ding, Y. H., and J. C. L. Chan, 2005: The East Asian summer monsoon: An overview. *Meteor. Atmos. Phys.*, **89**, 117–142.

Döscher, R., U. Willén, C. Jones, A. Rutgersson, H. E. M. Meier, U. Hansson, and L. P. Graham, 2002: The development of the regional coupled ocean–atmosphere model RCAO. *Boreal Environment Research*, **7**, 183–192.

Duchon, C. E., 1979: Lanczos filtering in one and two dimensions. *J. Appl. Meteor.*, **18**, 1016–1022.

Fang, Y. J., Y. C. Zhang, J. P. Tang, and X. J. Ren, 2010: A regional air–sea coupled model and its application over East Asia in the summer of 2000. *Adv. Atmos. Sci.*, **27**(3), 583–593, doi: 10.1007/s00376-009-8203-7.

Fu, C. B., H. L. Wei, and Y. Qian, 2000: Documentation on Regional Integrated Environmental Model System (RIEMS, Version I). TEACOM Science Report, No. 1, START Regional Committee for Temperate East Asia, Beijing, 38pp.

Fu, C. B., and Coauthors, 2005: Regional climate model intercomparison project for Asia. *Bull. Amer. Meteor. Soc.*, **86**, 257–266.

Fu, X., B. Wang, T. Li, and J. P. McCreary, 2003: Coupling between northward-propagating, intraseasonal oscillations and sea surface temperature in the Indian Ocean. *J. Atmos. Sci.*, **60**, 1733–1753.

Fu, X. H., B. Wang, and T. Li, 2005: Impacts of air–sea coupling on the simulation of mean Asian summer monsoon in the ECHAM4 model. *Mon. Wea. Rev.*, **130**, 2889–2904.

Giorgi, F., and G. T. Bates, 1989: The climatological skill of a regional model over complex terrain. *Mon. Wea. Rev.*, **117**(11), 2325–2347.

Grell, G. A., 1993: Prognostic evaluation of assumptions used by cumulus parameterization. *Mon. Wea. Rev.*, **121**, 764–787.

Holtslag, A. A. M., E. I. F. de Bruijin, and H. L. Pan, 1990: A high resolution air mass transformation model for short range weather forecasting. *Mon. Wea. Rev.*, **118**, 1561–1575.

Huang, R. H., and F. Y. Sun, 1994: Impacts of the thermal state and the convective activities in the tropical western warm pool on the summer climate anomalies in East Asia. *Chinese J. Atmos. Sci.*, **18**(2), 141–151. (in Chinese)

Huang, S. S., and Z. H. Yu, 1962: On the structure of the subtropical highs and some associated aspects of the general circulation of atmosphere. *Acta Meteorologica Sinica*, **31**, 339–359. (in Chinese)

Jiang, X., T. Li, and B. Wang, 2004: Structures and mechanisms of the northward propagating boreal summer intraseasonal oscillations. *J. Climate*, **17**, 1022–1039.

Kalnay, E., and Coauthors, 1996: The NCEP/NCAR 40-year reanalysis project. *Bull. Amer. Meteor. Soc.,* **77**, 437–471.

Kang, I. S., C. H. Ho, Y. K. Lim, and K. M. Lau, 1999: Principal modes of climatological seasonal and intraseasonal variations of the Asian summer monsoon. *Mon. Wea. Rev.*, **12**, 322–339.

Kim, J. E., and S. Y. Hong, 2007: Impact of soil moisture anomalies on summer rainfall over East Asia: A regional climate model study. *J. Climate*, **20**, 5732–5743.

Krishnamurti, T. N., 1985: Summer monsoon experiment —A review. *Mon. Wea. Rev.*, **113**, 1590–1626.

Lau, K. M., G. J. Yang, and S. H. Shen, 1988: Seasonal and intraseaonal climatology of summer monsoon rainfall over East Asia. *Mon. Wea. Rev.*, **116**, 18–37.

Lee, D. K., and M. S. Suh, 2000: Ten-year East Asian summer monsoon simulation using a regional climate model (RegCM2). *J. Geophys. Res.*, **105**(D24), 29565–29577.

Leung, L. R., S. J. Ghan, Z. C. Zhao, Y. Luo, W. C. Wang, and H. L. Wei, 1999: Intercomparison of regional climate simulations of the 1991 summer monsoon in eastern Asia. *J. Geophys. Res.*, **104**, 6425–6454.

Levitus, S., 1984: Annual cycle of temperature and heat storage in the world ocean. *J. Phys. Oceanogr.*, **14**, 727–746.

Li, T., and G. Q. Zhou, 2010: Preliminary results of a regional air–sea coupled model over East Asia. *Chinese Science Bulletin*, **55**, doi: 10.1007/s11434-010-0071-0.

Lin, A., T. Li, X. Fu, J. Luo, and Y. Masumoto, 2010: Effects of air–sea coupling on the boreal summer intraseasonal oscillations over the tropical

Indian Ocean. *Climate Dyn.*, **37**, 2303–2322, doi: 10.1007/s00382-010-0943-7.

Mao, J. Y., Z. Sun, and G. X. Wu, 2010: 20–50-day oscillation of summer Yangtze rainfall in response to intraseasonal variations in the subtropical high over the western North Pacific and South China Sea. *Climate Dyn.*, **34**, 747–761.

Mellor, G., and T. Yamada, 1982: Development of a turbulence closure model for geophysical fluid problems. *Rev. Geophys. Space Phys.*, **20**, 851–875.

Qian, Y. F., B. C. Zhu, and Q. Q. Wang, 1998: Computational scheme of horizontal pressure gradient in ocean models with σ coordinate system. *Journal of Nanjing University,* **34**(6), 691–700. (in Chinese)

Ratnam, J. V., F. Giorgi, A. Kaginalkar, and S. Cozzini, 2009: Simulation of the Indian monsoon using the RegCM3-ROMS regional coupled model. *Climate Dyn.*, **33**, 119–139.

Ren, X. J., and Y. F. Qian, 2005: A coupled regional air–sea model, its performances and climate drift in simulation of the East Asian summer monsoon in 1998. *Int. J. Climatol.,* **25**, 679–692.

Reynolds, R. W., N. A. Rayner, T. M. Smith, D. C. Stokes, and W. Q. Wang, 2002: An improved in situ and satellite SST analysis for climate. *J. Climate*, **15**, 1609–1625.

Seo, H., A. J. Miller, and J. Roads, 2007: The Scripps Coupled Ocean–Atmosphere Regional (SCOAR) Model, with applications in the eastern Pacific sector. *J. Climate*, **20**, 381–402.

Smagorinsky, J., 1963: General circulation experiments with the primitive equations. I. The basic experiment. *Mon. Wea. Rev.*, **91**, 99–164.

Tao, S., and L. Chen, 1987: A review of recent research on the East Asian summer monsoon in China. Review of monsoon meteorology, C. P. Chang and T. N. Krishnamurti, Eds., Oxford University Press, Oxford, 60–92.

Vincenzo, A., and Coauthors, 2010: An atmosphere–ocean regional climate model for the Mediterranean area: Assessment of a present climate simulation. *Climate Dyn.*, **35**, 721–740.

Wang, B., and X. Xu, 1997: Northern Hemisphere summer monsoon singularities and climatological intraseasonal oscillation. *J. Climate*, **10**, 1071–1085.

Wang, B., H. lin, Y. S. Zhang, and M. M. Lu, 2004: Definition of South China Sea monsoon onset and commencement of the East Asia summer monsoon. *J. Climate*, **17**(4), 699–710.

Wang, B., Q. H. Ding, X. H. Fu, I. S. Kang, K. Jin, J. Shukla, and D. R. Francisco, 2005: Fundamental challenge in simulation and prediction of summer monsoon rainfall. *Geophys. Res. Lett.*, **32**, L15711. doi: 10.1029/2005Gl022734.

Wang, Y. Q., O. L. Sen, and B. Wang, 2003: A highly resolved regional climate model (IPRC-RegCM) and its simulation of the 1998 severe precipitation event over China. Part I: Model description and verification of simulation. *J. Climate*, **16**, 1721–1738.

Wu, J., W. M. Jiang, C. B. Fu, B. K. Su, H. N. Liu, and J. P. Tang, 2004: Simulation studies of the radiative effect of black carbon aerosol and regional climate responses over China. *Adv. Atmos. Sci.*, **21**(4), 637–649, doi: 10.1007/BF02915731.

Wu, R., and B. P. Kirtman, 2007: Regimes of seasonal air–sea interaction and implications for performance of forced simulations. *Climate Dyn.*, **29**, 393–410.

Xie, P., and P. A. Arkin, 1997: Global precipitation: a 17-year monthly analysis based on gauge observations, satellite estimates, and numerical model outputs. *Bull. Amer. Meteor. Soc.*, **78**, 2539–558.

Xiong, Z., C. B. Fu, and Q. Zhang, 2006: On the ability of the regional climate model RIEMS to simulate the present climate over Asia. *Adv. Atmos. Sci.*, **23**(5), 784–791, doi: 10.1007/s00376-006-0784-9.

Yhang, Y. B., and S. Y. Hong, 2008: Improved physical processes in a regional climate model and their impact on the simulated summer monsoon circulations over East Asia. *J. Climate,* **21**, 963–979.

Zhang, Y. C., and Y. F. Qian, 1999: Numerical simulation of the regional ocean circulation in the coastal areas of China. *Adv. Atmos. Sci.*, **16**(3), 443–450, doi: 10.1007/s00376-999-0022-3.

Zou, L. W., and T. J. Zhou, 2011: Sensitivity of a regional ocean–atmosphere coupled model to convection parameterization over western North Pacific. *J. Geophys. Res.*, **116**, D18106, doi: 10.1029/2011JD015844.

Zou, L. W., T. J. Zhou, Z. X. Li, and J. Zhang: 2010: East China summer rainfall variability of 1958–2000: Dynamical downscaling with a variable-resolution AGCM. *J. Climate*, **23**, 6394–6408.